Virtual inflow monitoring for a three phase gravity separator*

Christoph Josef Backi and Sigurd Skogestad

Abstract— **This paper presents a virtual monitoring approach for a gravity separator. It is used to separate the three phases oil, water and gas. The monitored variables are thereby the gaseous and liquid inflows as well as the effective split ratio of oil and water entering the continuous water phase. Measurements for these variables are either expensive, unreliable or even impossible to take (as for the split ratio). Therefore, an Extended Kalman Filter is designed, which can estimate the inflows and the split factor based on a model of the dynamic system. The performance is shown in simulations, where the gravity separator's states are controlled by PI controllers.**

I. INTRODUCTION

The separation of phases such as hydrocarbons (oil and condensate), gas and water from a well stream is crucial in subsea production facilities to obtain as pure single phase streams as possible. These can be distributed further by standard single phase pumps and compressors. In general, a first rough separation stage can thereby be a gravity separator, which relies on separation by mainly gravitational forces and density differences between the respective phases. Hence, oil droplets dispersed in the continuous water phase will rise towards the continuous oil phase, while water droplets will settle through the continuous oil phase towards the continuous water phase.

In order to operate the gravity separator within specified limits, it is crucial to control the state variables (water and overall liquid levels as well as gas pressure) to nominal values. We use simple PI control algorithms relying on the estimated values of the level and pressure measurements. For monitoring purposes it is beneficial to obtain more information about the process conditions, for example the inflows of gas and liquid as well as the split ratio of oil and gas entering the continuous water phase. Hence, a state and parameter observer will be designed to estimate these values and to obtain less noisy signals of the measured variables for control purposes. A suitable design for such an observer is an Extended Kalman Filter (EKF), which has been and is still used in a broad variety of applications due to its simplicity and robustness properties.

One of the reasons to use an observer to determine the inflows of liquid and gas as well as the (effective) split ratio is the rather poor accuracy of multiphase flowmeters as well as of measurement devices to determine the fraction of oil in water or water in oil. Several methods have been proposed for the latter, where [12] report about a method using low-field nuclear magnetic resonance (NMR) to determine the droplet size distribution in water-in-oil emulsions. They conclude that the correlation between the method and a reference technique (optical microscope) was good and that the advantage of the introduced method was the determination of the droplet size distribution without making assumptions on its shape. Another method is the so called electrical resistance tomography (ERT), as described and applied in e.g. [2], [3] and [9]. The principle behind this method is an array of probes mounted to a pipe acting as both transmitter and receiver. Typically, one probe transmits a current signal while all other probes act as receivers one after another. Then the next probe acts as transmitter, and so on. If this is done continuously, one can calculate the resistance active between two probes and thus calculate the composition of the medium. This however only holds for certain flow regimes and hence calibration might be difficult. A differential dielectric sensor model and its applications for water and oil flow is introduced by [5]. The authors conclude that it agrees very well with test data, however, only for specific, well-mixed, homogeneous fluids. In their brief article, [6] describe energy dispersive x-ray scatter for measurement of oil/water ratios and conclude that the methodology has great potential for multiphase flow measurement and on-line monitoring. Multiphase flowmeters are generally expensive and require high maintenance. An overview on multiphase flow metering technology is provided in [11].

Other measurements needed in separation devices are level measurements for oil and water interface determination. A single-electrode capacitance probe is introduced in [4], which assumes clear interfaces. However, this has disadvantages in spatial resolution and therefore segmented probes consisting of an array of identical measurement devices can be used, such as the segmented capacitance interface probe. An ultrasonic-based device for accurate measurement of oil, emulsion and water levels is presented in [8]. The authors conclude that using ultrasound for this application is not only reasonable from a physics point of view, but also from an integrated electronics point of view. In industry, often so-called nucleonic level measurements are used, which provide density measurements and hence interface locations together with phase levels can be determined, see e.g. [7].

In general, bad calibration, sensor drift and measurement noise impose high restrictions and requirements on the measurement and monitoring devices introduced above. Hence, not only the modeling part is crucial in order to perform satisfying control tasks, but also the measurement devices.

The paper is structured as follows: In Section II the

*This work was supported by the Norwegian Research Council under the project SUBPRO (Subsea production and processing)

C. J. Backi (corresponding author) and S. Skogestad are with the Department of Chemical Engineering, Norwegian University of Science and Technology, N-7491 Trondheim, Norway {christoph.backi,sigurd.skogestad}@ntnu.no

mathematical model for a gravity separator is introduced, while in Section III the observer and controller design is presented. Section IV gives the simulation results, whereas Section V closes the paper with the conclusion.

II. MATHEMATICAL MODEL

The process that is modeled is a gravity separator depicted in Figure 1. It has the shape of a long cylinder, where at the left side the oil-water-gas mixture is fed into the separator. A first rough separation occurs due to turbulence, hence continuous water and oil layers are formed. For simplicity, it is assumed that the gas is immediately flashed out of the liquid phases, hence there are no gas bubbles in the liquid phases. Furthermore, it is assumed that there are no liquid droplets in the continuous gas phase. The inlet zone is followed by the so-called active separation zone, where droplets rise or settle to their respective bulk phases due to density differences. Other phenomena like coalescence (small droplets form a big droplet) or breakage (smaller droplets are formed out of a big droplet) can occur as well. On the right-hand side, the outlet zone can be found, where the gas, water and oil phases are released from the separator. Other assumptions include the absence of a dense-packed (emulsion) layer between the continuous oil and water layers as well as an average velocity for the respective oil and water layers including the dispersed droplets.

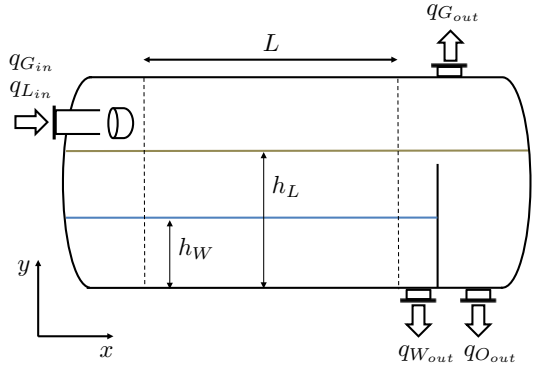

Fig. 1. Simplified schematic of the gravity separator

A. Dynamic part

The mathematical model that is used for controller and observer design in Section III was introduced in detail in [1] and is shown here for completeness. The model consists of three dynamic states, namely the overall liquid level h_L (oil plus water), the water level h_W and the gas pressure p. Note that the simplifications of the trogonometric functions in (1) and (2) were not included in [1].

The in- and outflow dynamics for the water and liquid levels result in the following differential equations:

$$\begin{aligned}\frac{dh_L}{dt} &= \frac{dV_L}{dt}\frac{\sqrt{h_L(2r-h_L)}}{r^2L\left(1-\cos\left(2\arccos(\frac{r-h_L}{r})\right)\right)} \\ &= \frac{dV_L}{dt}\frac{1}{2L\sqrt{h_L(2r-h_L)}},\end{aligned} \tag{1}$$

$$\begin{aligned}\frac{dh_W}{dt} &= \frac{dV_W}{dt}\frac{\sqrt{h_W(2r-h_W)}}{r^2L\left(1-\cos\left(2\arccos(\frac{r-h_W}{r})\right)\right)} \\ &= \frac{dV_W}{dt}\frac{1}{2L\sqrt{h_W(2r-h_W)}},\end{aligned} \tag{2}$$

where r is the radius of the gravity separator and L denotes length of the active separation zone, as well as the change of volumes

$$\frac{dV_L}{dt} = q_{L,in} - q_{L,out} = q_{L,in} - q_{W,out} - q_{O,out}, \tag{3}$$

$$\frac{dV_W}{dt} = q_{W,in} - q_{W,out} = q_{L,in}(\alpha\phi_{ww} + \beta\phi_{ow}) - q_{W,out}, \tag{4}$$

where α is the water cut, $\beta = 1-\alpha$ indicates the oil cut, q_i denote in- or outflows of either liquid (L), water (W) or oil (O) and ϕ_{ww} as well as ϕ_{ow} represent the fractions of inflowing water and oil directly going into the continuous water phase (indices *ww* and *ow*, respectively).

The pressure dynamics are derived from the ideal gas law assuming constant temperature

$$\frac{dp}{dt}(V_{Sep} - V_L) = RT\frac{\rho_G}{M_G}(q_{G,in} - q_{G,out}) + p\,(q_{L,in} - q_{L,out}) \tag{5}$$

with volume of the active separation zone V_{Sep}, liquid volume

$$V_L = \frac{r^2L}{2}\left[2\arccos\left(\frac{r-h_L}{r}\right) - \sin\left(2\arccos\left(\frac{r-h_L}{r}\right)\right)\right],$$

universal gas constant R, temperature T, density of gas ρ_G and the in- and outflows of gas (G) or liquid (L), respectively.

The controlled (manipulated) variables are the outflows of oil $q_{O,out}$, water $q_{W,out}$ and gas $q_{G,out}$. The disturbance variables to the model are the inflow of liquid $q_{L,in}$ (sum of the inflows of water and oil), the inflow of gas $q_{G,in}$ as well as the split ratio γ of liquid (water and oil) entering the continuous water phase (compare to (4))

$$\gamma = \alpha\phi_{ww} + \beta\phi_{ow} = \alpha\,(1-\phi_{wo}) + (1-\alpha)\,\phi_{ow}.$$

B. Static part

In addition to the dynamic part described above, the model consists of a static part, namely calculations of droplet distributions throughout the respective continuous phases in the active separation zone. Thereby, the horizontal residence time of a droplet size class is compared to its vertical residence time, meaning the time a droplet size class needs to reach the oil-water-interface. The horizontal residence time is calculated using the horizontal velocity of the oil and water phases (inflow of oil and water divided by the respective cross-sectional areas), whereas the vertical residence time is calculated using Stokes' law, which gives a vertical velocity for a droplet dispersed in a continuous phase. More details on the static part can be found in [1].

III. CONTROLLER DESIGN

We are going to introduce the conttoller and observer design to control the gravity separator's dynamic states, namely the liquid and water levels, h_L and h_W, as well as the pressure p as well as to estimate the disturbance variables and parameters $q_{L,in}$, $q_{G,in}$ and γ.

A. Observer Design

Figure 2 shows a schematic of the Extended Kalman Filter together with the model of the plant representing the real system. The EKF shown in the dashed rectangle is provided with the manipulated variables $q_{O,out}$, $q_{W,out}$ and $q_{G,out}$ as well as the measured variables h_L, h_W and p and delivers the estimated outputs $\hat{h}_L$, $\hat{h}_W$ and $\hat{p}$ as well as the disturbance variables $\hat{q}_{L,in}$, $\hat{q}_{G,in}$ and $\hat{\gamma}$.

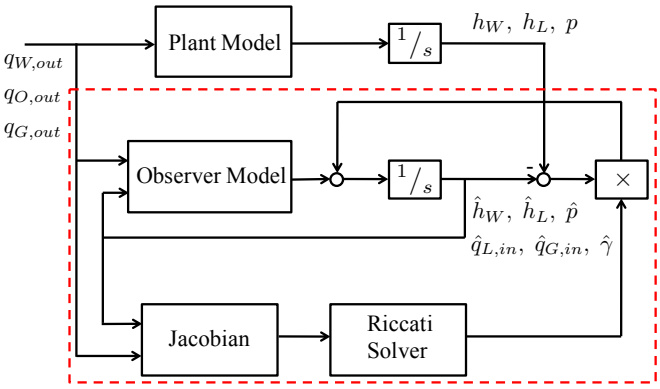

Fig. 2. Schematic of the Extended Kalman Filter (dotted red area) in combination with the plant model

The block 'Plant Model' is composed of equations (1)–(5). The block 'Observer Model' consists of the following state equations

$$\begin{aligned}
\frac{d\hat{h}_L}{dt} &= f_1 = \frac{\hat{q}_{L,in} - q_{W,out} - q_{O,out}}{2L\sqrt{\hat{h}_L(2r-\hat{h}_L)}},\\
\frac{d\hat{h}_W}{dt} &= f_2 = \frac{\hat{q}_{L,in}\hat{\gamma} - q_{W,out}}{2L\sqrt{\hat{h}_W(2r-\hat{h}_W)}},\\
\frac{d\hat{p}}{dt} &= f_3 = \frac{RT\frac{\rho_G}{M_G}(\hat{q}_{G,in} - q_{G,out}) + \hat{p}\,(\hat{q}_{L,in} - q_{L,out})}{V_{Sep} - \hat{V}_L},
\end{aligned} \tag{6}$$

where $\hat{V}_L$ denotes the liquid volume calculated with the estimated level $\hat{h}_L$. Furthermore, all three state variables are assumed to be measurable. In addition to the state variables introduced above, we define three more states representing disturbance variables and parameters, respectively. These are $\hat{q}_{L,in}$, $\hat{q}_{G,in}$ and $\hat{\gamma}$ with their respective dynamics:

$$\frac{d\hat{q}_{L,in}}{dt} = f_4 = 0, \quad \frac{d\hat{q}_{G,in}}{dt} = f_5 = 0, \quad \frac{d\hat{\gamma}}{dt} = f_6 = 0. \tag{7}$$

Let us define the vector of state-estimates as

$$\hat{x} = \begin{bmatrix}\hat{h}_L & \hat{h}_W & \hat{p} & \hat{q}_{L,in} & \hat{q}_{G,in} & \hat{\gamma}\end{bmatrix}^T.$$

The block 'Observer Model' does not include the static part as introduced in Section II-B in order to regard for some mismatch between plant and observer in simulations and due to the fact that this information would not be available from a real plant.

In the block 'Jacobian' the partial derivatives of the observer state equations (6)–(7) with respect to the state vector $\hat{x}$ are computed and updated at every time iteration. The single entries in the Jacobian A give complicated terms, but its shape is

$$\begin{aligned}
A_O(t) &= \left(\frac{\partial f_i}{\partial \hat{x}_j}\right)_{i=1,\dots,6;\ j=1,\dots,6}\\
&= \begin{bmatrix}
\begin{bmatrix} A_O^{11}(t) & 0 & 0\\ 0 & A_O^{22}(t) & 0\\ A_O^{31}(t) & 0 & A_O^{33}(t)\end{bmatrix} & \begin{bmatrix} A_O^{14}(t) & 0 & 0\\ A_O^{24}(t) & 0 & A_O^{26}(t)\\ A_O^{34}(t) & A_O^{35}(t) & 0\end{bmatrix}\\
0_{(3\times 3)} & 0_{(3\times 3)}
\end{bmatrix}.
\end{aligned} \tag{8}$$

It is further used to solve the differential Matrix-Riccati-Equations in the block 'Riccati Solver' to calculate the time-varying Kalman feedback gain matrix $K_O(t)$

$$\begin{aligned}
\dot{P}(t) &= A_O(t)P(t) + P(t)A_O^T(t) - P(t)C_O^T R_O^{-1} C P(t) + Q_O,\\
K_O(t) &= P(t)C_O^T R_O^{-1},
\end{aligned}$$

where the output matrix is defined as

$$C_O = \begin{bmatrix} 1 & 0 & 0 & 0 & 0 & 0\\ 0 & 1 & 0 & 0 & 0 & 0\\ 0 & 0 & 1 & 0 & 0 & 0\end{bmatrix} \tag{9}$$

and $Q_O = \mathrm{cov}\{w(t)w^T(t)\} = \mathrm{diag}\,(q_{O,i})$, $i = 1,\dots,6$, is the covariance of the process noise and $R_O = \mathrm{cov}\{v(t)v^T(t)\} = \mathrm{diag}\,(r_{O,k})$, $k = 1,\dots,3$, is the covariance of the measurement noise. No covariance is assumed between the process and the measurement noises, which are assumed to enter the system in the following way

$$\begin{aligned}
\frac{d\hat{x}}{dt} &= A_O\hat{x} + B_O u + \Gamma w(t),\\
y &= C_O\hat{x} + D_O u + v(t),
\end{aligned}$$

with $\Gamma = I_{(6\times 6)}$, $D_O = 0_{(3\times 3)}$, $u = \begin{bmatrix} q_{O,out} & q_{W,out} & q_{G,out}\end{bmatrix}^T$ and the input matrix

$$B_O(t) = \left(\frac{\partial f_i}{\partial u_m}\right)_{i=1,\dots,6;\ m=1,\dots,3} = \begin{bmatrix} B_O^{11}(t) & B_O^{12}(t) & 0\\ 0 & B_O^{22}(t) & 0\\ B_O^{31}(t) & B_O^{32}(t) & B_O^{33}(t)\end{bmatrix}. \tag{10}$$

The observability condition states that the observability matrix $\mathcal{O} = \begin{bmatrix} C_O\\ C_O A_O(t)\\ \vdots\\ C_O A_O(t)^{n-1}\end{bmatrix}$ for $n = 6$ must have full rank for all t. For the matrix $A_O(t)$ in the shape as presented in (8), $\mathrm{rank}\,(\mathcal{O}) = 6$ and hence full observability is ensured. A further investigation of the matrix $A_O(t)$ for steady-state conditions, meaning that inflows equal outflows, lead to the Jacobian

$$A_O^{\text{steady}}(t) = \begin{bmatrix} & \begin{bmatrix} A_O^{14}(t) & 0 & 0 \\ A_O^{24}(t) & 0 & A_O^{26}(t) \\ A_O^{34}(t) & A_O^{35}(t) & 0 \end{bmatrix} \\ 0_{(3\times3)} & \\ & 0_{(3\times3)} \end{bmatrix}, \quad (11)$$

which, for the output matrix (9) still leads to $\text{rank}(\mathcal{O}) = 6$. The only cases that could potentially lead for any of the remaining entries in (11) to be zero, are $h_L \equiv 2r$, $h_W \equiv 2r$ and $V_L \equiv V_{Sep} \Rightarrow V_G \equiv 0$. However, the model is not designed for these cases and they are unlikely to happen in normal operation. Hence, it can be concluded that the model is fully observable for any feasible operational setpoint.

B. PI Controller

The PI control laws are defined in the form

$$K(s) = K_p + T_I \frac{1}{s},$$

where the parameters K_p and T_I are shown in Table I. The parameters of the PI controllers are the same as already presented in [1] and were found by applying the SIMC tuning rules, as suggested in [10]. Therein, the only tuning parameter τ_c of the SIMC tuning rules is discussed in detail. The chosen values of τ_c for the three PI controllers are also shown in Table I.

The PI controllers do not use the noisy measurements of the state variables, but the filtered ones delivered by the estimator. The rates of change for controller action are limited to ± 0.05 m^3 s^{-2} and their outputs are lower and upper bounded at 0 and 1 m^3 s^{-1}, respectively.

TABLE I

PARAMETERS FOR THE THREE PI CONTROLLERS

	τ_c	K_P	T_I
water level	5 s	≈ 6.49	≈ 0.325
liquid level	3 s	≈ 8.44	≈ 0.7
pressure	5 s	≈ 0.0541	≈ 0.0027

IV. SIMULATION RESULTS

In this Section, some results of simulation studies are presented, which shall demonstrate the capabilities of the disturbance estimation. We will show that robustness with respect to particular disturbances in the form of white Gaussian noise can be handled satisfyingly. At $t = 200$ s, $t = 400$ s and $t = 600$ s, step changes in the water level of $+0.2$ m occur, whereas the liquid level is held constant. At $t = 400$ s and $t = 600$ s, step changes of $+0.1$ m^3 s^{-1} for the liquid and gas inflows are introduced.

In simulations, the pressure state (5) is scaled to the unit bar in the following way, hence the equation used for the plant as well as for the observer model is

$$\frac{dp}{dt} = 10^{-5} \left(\frac{RT \frac{\rho_G}{M_G} (q_{G,in} - q_{G,out}) + 10^5 p (q_{L,in} - q_{L,out})}{V_{Sep} - V_L} \right).$$

A. Results with added noise to the disturbances

In this Section, results for added white Gaussian noise to the disturbances $q_{L,in}$ and $q_{G,in}$ are presented. Figure 3 shows that the water level h_W is brought to the new nominal values after step changes in the desired value have been introduced. Furthermore, it can be seen that the other state variables remain at their desired values after a short settling time in the beginning of the simulation. The control action can be seen in the bottom plot of Figure 3. In addition, the plots show that, since all state variables are assumed measurable, their estimates converge quickly to the real values. There is some noisy behavior in the beginning of the simulation for the pressure state estimate, which is caused by the tuning of the observer aiming for performance of the disturbance estimation. The step changes in the inflows of liquid and gas at $t = 400$ s and $t = 600$ s are handled well by the controllers.

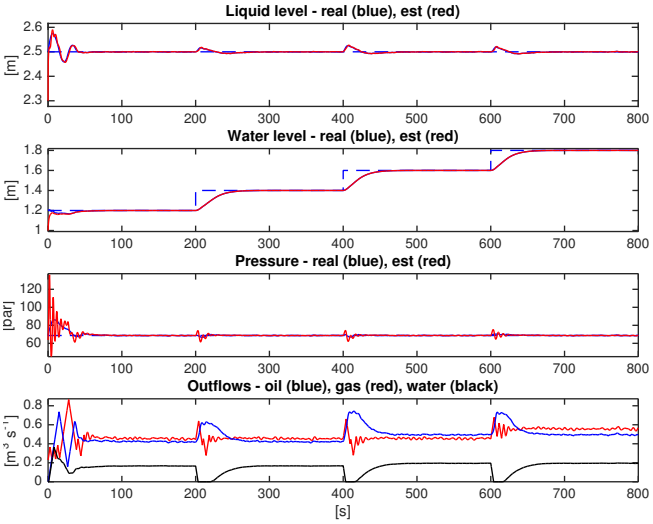

Fig. 3. Top three plots: real (blue) and estimated (red) state variables together with setpoints (dashed blue); bottom plot: outflows for water (black), oil (blue) and gas (red) over time

In Figure 4 the estimated inflows and the fraction of oil and water going into the continuous water phase are presented. As can be seen in the top plot, the estimated liquid inflow reaches its nominal value substantially faster than the inflow of gas. However, both estimates track their nominal values. A substantial difference between real and estimated value of the parameter γ can be seen in the bottom plot. This is caused by the static droplet calculations (Section II-B), which are included in the plant, but not in the observer model. The volumetric oil flow leaving the continuous water phase is larger than the volumetric water flow leaving the continuous oil phase and hence, in steady-state, the estimated value for γ is smaller than the real value as there is a net outflow from the continuous water phase.

B. Results with added measurement noise

This Section presents simulation results for white Gaussian noise directly added to the measured variables. In Figure 5

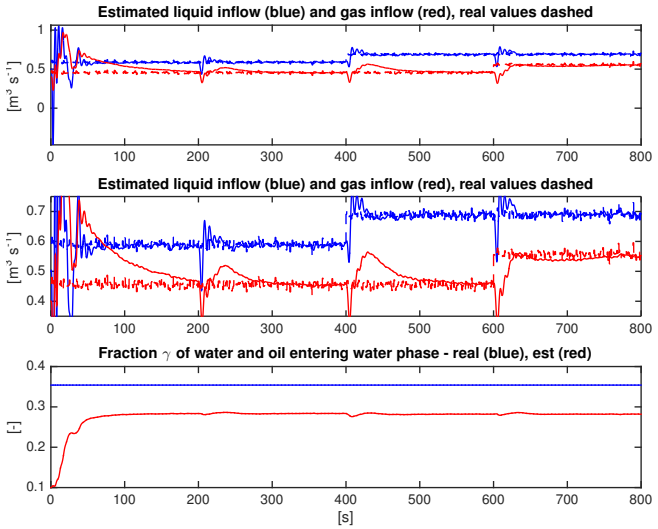

Fig. 4. Top plot: real (dashed) and estimated (solid) variables, liquid inflow (blue) and gas inflow (red); center plot: zoom of top plot; bottom plot: real (blue) and estimated (red) split ratio γ

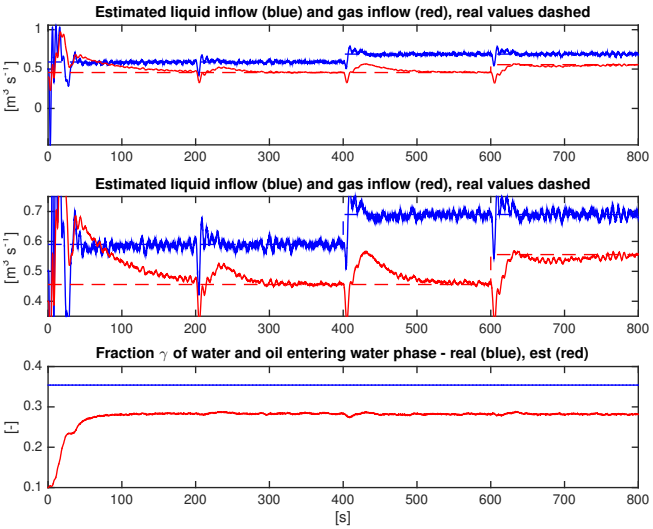

Fig. 6. Top plot: real (dashed) and estimated (solid) variables, liquid inflow (blue) and gas inflow (red); center plot: zoom of top plot; bottom plot: real (blue) and estimated (red) split ratio γ

the noise in the measurements is clearly visible. However, the observer is able to track the real values and deliver filtered signals to the controller. Like already shown in Figure 3, after a short settling time in the beginning of the simulation, the states are held at their desired values.

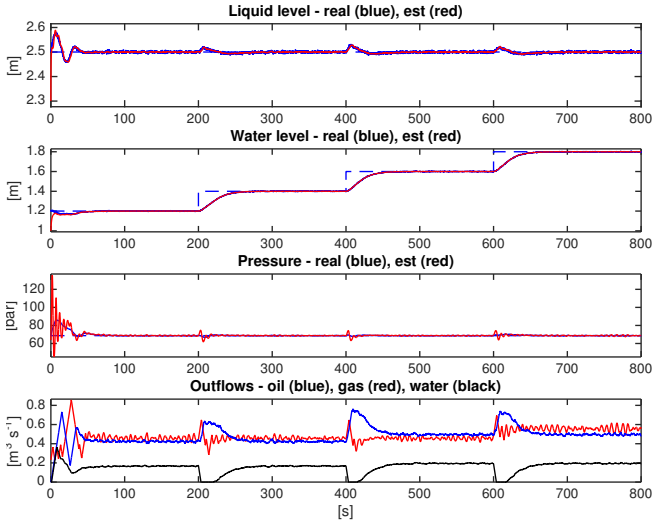

Fig. 5. Top three plots: real (blue) and estimated (red) state variables together with setpoints (dashed blue); bottom plot: outflows for water (black), oil (blue) and gas (red) over time

In Figure 6, like in Figure 4, the estimated liquid and gas inflows are shown. The introduction of the measurement noise is clearly visible in the disturbance estimates, especially for the the liquid inflow. Despite the noisier behavior, the observer is able to track the nominal inflows correctly. In the bottom, plot the estimated parameter $\hat{\gamma}$ is presented with the same deviation from the real value as already shown in the bottom plot of Figure 4.

C. Results with added noise to the disturbances and measurements

In this simulation case, we combine the two studies in Sections IV-A and IV-B to obtain an even more realistic picture with added noise to both measurements and disturbances.

The state estimation and controller performance did not change much compared to Figure 5 and therefore the plot showing the states and their estimates as well as the manipulated variables is not shown here due to space limitations. Figure 7 shows the estimated inflows together with their respective noisy reference values (dashed lines). The noise level of the parameter estimates is slightly larger compared to the previous simulations. The noise introduced by the measurements seems to be more dominant than that added to the disturbance variables, especially for the liquid inflow. The bottom plot presents the estimated parameter $\hat{\gamma}$ with the same deviation from the real value as in earlier simulations.

V. CONCLUSION

In this paper, we presented a virtual monitoring approach for the inflows and the effective split ratio of oil and water entering the continuous water phase in a gravity separator. An Extended Kalman Filter was used to filter the signals of the measured state variables (liquid and water levels as well as gas pressure) and to obtain estimates for the disturbance variables (liquid and gas inflows) acting on the process as well as the effective split ratio. Simple PI control algorithms were used to control the state variables and tuned by the SIMC tuning rules.

The performance of the Extended Kalman Filter together with the PI controllers is presented for different simulation cases. These include tracking of step changes in the desired water level as well disturbance compensation introduced as step changes in the inflows of liquid and gas, respectively.

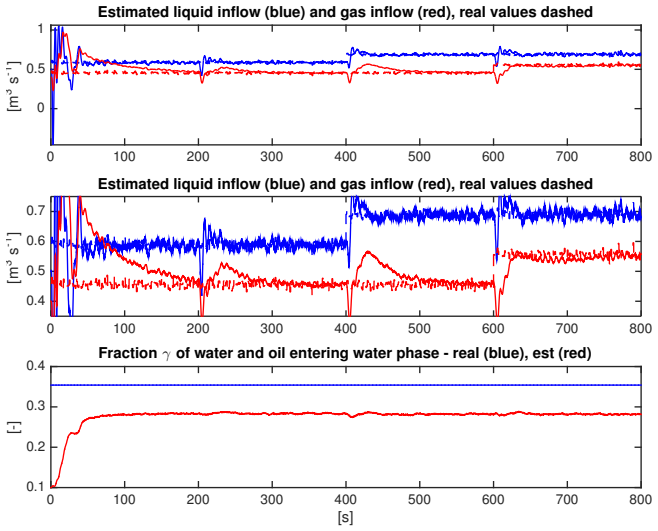

Fig. 7. Top plot: real (dashed) and estimated (solid) variables, liquid inflow (blue) and gas inflow (red); center plot: zoom of top plot; bottom plot: real (blue) and estimated (red) split ratio γ

In addition, white noise was added to the three measured state variables as well as to the disturbance variables. The simulation results show that the proposed control and estimation structure is capable of estimating smoother values of the state variables and utilize these in the controllers. In addition, the nominal values of the disturbance variables are estimated correctly. However, after introducing noise, especially to the measurements, the disturbance estimates become quite noisy as well.

The only drawback of the estimation and control structure is that the split ratio γ of oil and water entering the continuous water phase cannot be estimated correctly. This, however, is caused by the fact that there is a net outflow of oil leaving the continuous water phase into the continuous oil phase due to steady-state separation calculations introduced in Section II-B. This static part of the model is included in the plant, but not in the observer. Hence, the estimated value $\hat{\gamma}$ represents the effective split ratio in steady-state conditions including separation.

The suggested estimation and control structure is not limited to separation systems in the oil and gas industry, but can be implemented in all kinds of in- and outflow systems. Nevertheless, in order to prove its value and implementability, it should be tested on a real plant, preferably for a single-phase application in the beginning.

Future work can include further investigation of the deviation between the split ratio γ and its estimated value $\hat{\gamma}$ and how to utilize this information in a real application. The split ratio itself is not determinable, but a qualitative interpretation of its estimate could lead to a better understanding of the separation inside the separator. In addition, obtaining less noisy disturbance estimates could lead to the design of more sophisticated control structures including these estimates in a feedforward-manner with disturbance compensation by state-feedback control. This can either be achieved by improved tuning of the Extended Kalman Filter or by additionally applying low-pass filters to the estimates. Some preliminary work in this direction has already been done by the authors.

APPENDIX: SIMULATION PARAMETERS

$$Q_O = \mathrm{diag}\left(10^{-1},\quad 10^{-1},\quad 10^{-1},\quad 10^{1},\quad 10^{0},\quad 10^{0}\right)$$
$$R_O = \mathrm{diag}\left(10^{-1},\quad 10^{0},\quad 10^{4}\right)$$

L	Length (active separation zone)	10 m
M_G	Molar mass of the gas	0.01604 kg mol^{-1}
r	Radius of the separator	1.65 m
R	Universal gas constant	8.314 $\frac{\text{kg m}^2}{\text{s}^2\ \text{mol K}}$
T	Temperature	328.5 K
V_{Sep}	(Volume active separation zone)	85.53 m^3
$q_{G,in}$	Volumetric inflow of gas	0.456 m^3 s^{-1}
$q_{L,in}$	Volumetric inflow of liquid	0.59 m^3 s^{-1}
α	Water cut of the liquid inflow	0.135
γ	Split ratio	0.354
ρ_G	Density of gas	49.7 kg m^{-3}
ϕ_{wo}	Initial water to oil fraction	0.3
ϕ_{ow}	Initial oil to water fraction	0.3

REFERENCES

[1] C. J. Backi and S. Skogestad. A simple dynamic gravity separator model for separation efficiency evaluation incorporating level and pressure control. In *Proceedings of the 2017 American Control Conference*, Seattle, USA, May 24–26 2017.

[2] M. A. Bennett and R. A. Williams. Monitoring the operation of an oil/water separator using impedance tomography. *Minerals Engineering*, 17:605–614, 2004.

[3] P. Durdevic, L. Hansen, C. Mai, S. Pedersen, and Z. Yang. Cost-Effective ERT Technique for Oil-in-Water Measurement for Offshore Hydrocyclone Installations. In *Proceedings of the 2nd IFAC Workshop on Automatic Control in Offshore Oil and Gas Production*, pages 153–159, Florianópolis, Brazil, May 2015.

[4] A. J. Jaworski and G. Meng. On-line measurement of separation dynamics in primary gas/oil/water separators: Challenges and technical solutions – A review. *Journal of Petroleum Science and Engineering*, 68:47–59, 2009.

[5] H. Li, R. S. Mohan, J. Marrelli, and S. Wang. Differential Dielectric Sensor Model and Its Applications for Water and Oil Flow. In *Proceedings of the ASME 2010 International Mechanical Engineering Congress & Exposition (IMECE 2010)*, Vancouver, BC, Canada, November 12–18 2010.

[6] R. D. Luggar, M. J. Key, E. J. Morton, and W. B. Gilboy. Energy dispersive X-ray scatter for measurement of oil/water ratios. *Nuclear Instruments and Methods in Physics Research A*, 422:938–941, 1999.

[7] O. T. McClimans and R. Fantoft. Status and New Developments in Subsea Processing. In *Proceedings of the 2006 Offshore Technology Conference*, Houston, TX, USA, May 1–4 2006.

[8] M. Meribout, M. Habli, A. Al-Naamany, and K. Al-Busaidi. A New Ultrasonic-based Device for Accurate Measurement of Oil, Emulsion, and Water Levels in Oil Tanks. In *Proceedings of the 2004 Instrumentation and Measurement Technology Conference*, Como, Italy, May 18–20 2004.

[9] S. Pedersen, C. Mai, L. Hansen, P. Durdevic, and Z. Yang. Online Slug Detection in Multi-Phase Transportation Pipelines Using Electrical Tomography. In *Proceedings of the 2nd IFAC Workshop on Automatic Control in Offshore Oil and Gas Production*, pages 165–170, Florianópolis, Brazil, May 2015.

[10] S. Skogestad. Simple analytic rules for model reduction and PID controller tuning. *Journal of Process Control*, 13:291–309, 2003.

[11] R. Thorn, G. Johansen, and B. Hjertaker. Three-phase flow measurement in the petroleum industry. *Measurement Science and Technology*, 24(1), 2013.

[12] N. van der Tuuk Opedal, G. Sørland, and J. Sjöblom. Methods for Droplet Size Distribution Determination of Water-in-Oil Emulsions using Low-Field NMR. *diffusion-fundamentals.org*, 9(7):1–29, 2009.